Crack layer analysis of fatigue fracture of poly(ethylene terephthalate)

J. Krey and K. Friedrich
Polymer and Composite Group, Technical University Hamburg–Harburg, 2100 Hamburg 90, FRG

and A. Moet*
Department of Macromolecular Science, Case Western Reserve University, Cleveland, Ohio 44106-2699, USA
(Received 11 December 1987; accepted 5 January 1988)

In this study a systematic characterization of the kinetics and mechanics of fatigue crack propagation in crystalline poly(ethylene terephthalate) is presented. It is shown that the crack is accompanied by a large zone of transformed material. Based on the crack layer theory, the data of fatigue crack propagation are analysed. According to this theory, the specific enthalpy of damage is a material parameter, which is found to be about 2000 kJ m^{-3}. Also, a detailed description of the method of data analysis with respect to the crack layer theory is given.

(Keywords: fatigue; poly(ethylene terephtalate); crack layer; specific enthalpy)

INTRODUCTION

The crack propagation behaviour in amorphous and crystalline poly(ethylene terephthalate) (PET) is discussed in recent literature[1,2]. In both cases the crack growth rate is described as a function of the stress intensity factor range ΔK. Over a limited range of ΔK the Paris equation[3]:

$$dl/dN = A(\Delta K)^m \quad (1)$$

is believed to be valid. A log–log plot of the rate of crack propagation dl/dN vs. the stress intensity factor range is suggested to yield a straight line with a slope of m and an intercept of A. The parameters A and m are empirical characteristics of the resistance to crack propagation. The Paris equation is based on the concepts of linear elastic fracture mechanics, and characterizes a rectilinear crack by a single parameter, the crack length.

However, in most polymers, including PET[1,2], the crack tip is surrounded by a zone of damaged material. The crack layer theory[4,5] describes the crack propagation resistance in terms of material transformation preceding the crack tip, i.e. active zone. The material transformation in this zone consumes energy and thus constitutes the major source of resistance to crack growth[6–8].

In this study a systematic characterization of the kinetics and mechanics of fatigue crack propagation (FCP) in crystalline PET is presented. On the basis of the crack layer theory, the material's behaviour with respect to the large amount of transformed material around the crack tip is described. A detailed description of the method of data analysis is also given.

* To whom correspondence should be addressed

EXPERIMENTAL

Material

The material used in this investigation is a semi-crystalline PET modified by 20% ionomeric particles (E.I. du Pont de Nemours & Co. Inc., Wilmington, USA). The specimens were provided as injection-moulded, rectangular plaques (*Figure 1*). The mechanical properties were determined from a tensile test (*Figure 2a*) conducted in a Zwick 1445 at a crosshead speed of 0.5 mm min^{-1} at room temperature. The mechanical properties and the density are listed in *Table 1*[9,10].

A two-phase model is invoked[11] for calculating the degree of crystallinity from density data. The crystalline and amorphous densities were taken as[12] 1.445 and 1.335 g cm^{-3}, respectively. In addition, d.s.c. measurements of the virgin material were made. The results of both methods are listed in *Table 2*.

Fatigue crack propagation test

A 60° angular notch of 1 mm depth and an additional razor-blade notch of 1 mm depth were introduced into rectangular specimens to produce an initial notch length of 2 mm. A schematic of the specimen geometry is shown in *Figure 2b*. Fatigue crack propagation tests were conducted on an MTS servohydraulic machine using a sinusoidal waveform at a frequency of 1 Hz. The loading was tension–tension with a maximum stress of 11 MPa and a minimum-to-maximum load ratio of 0.2. The evolution of the crack and the surrounding damage zone were monitored with a travelling microscope, which was attached to a video-camera assembly. To improve the contrast, the sides of the samples were polished and coated with a thin layer of gold. The load–displacement

0032-3861/88/081433-08$03.00

curves were recorded on an x–y chart recorder and also stored in an IBM PC computer. The program calculated and stored the irreversible work and the potential energy during crack propagation. Estimations of crack growth rate and active zone evolutions were taken from video playbacks.

Microscopy

By using an optical stereomicroscope and reflected light, the fracture surface profile and damage zone widths were studied. Thin sections perpendicular to the fracture surface were prepared by metallographic grinding and polishing procedures, and examined using transmitted light on an optical microscope. The fracture surfaces were also examined with a Jeol scanning electron microscope to obtain further information about the fracture mechanisms. For this procedure, the fracture surfaces were coated with a layer of gold–palladium.

CRACK LAYER THEORY

In its general form, the crack layer (CL) theory considers a fracture process as the propagation of a layer of damaged material around the main crack (*Figure 3*). The region in front of the actual crack tip where material transformation takes place is called the 'active zone'. This zone is limited by its trailing and leading edges, and is characterized by its width (w) and its length (l_a). Three elementary movements describe the motion of the active zone: translation, expansion and distortion. The law of active zone translation during fatigue crack propagation is derived as[5,6]:

$$\frac{dl}{dN} = \frac{\beta}{(\gamma^* R_t - A_1) t_0} \frac{dW_i}{dN} \tag{2}$$

where dl/dN is the crack growth rate, dW_i/dN is the total irreversible work done per cycle on damage and heat evolution within the active zone. β is a proportionality coefficient, which expresses the portion of irreversible work expended on damage formation within the active zone, γ^* is the specific enthalpy of damage, R_t is the translational resistance moment, A_1 is the total energy

Table 1 Mechanical properties of crystalline PET used in this study

Density, ρ (g cm^{-3})	Yield stress, α_y (MPa)	Modulus, E (MPa)	Elongation to fracture, ε (%)	Poisson's ratio, ν
1.37	26.5	1650	110	0.43

Table 2 Crystallinity of the virgin material and damaged material

	Crystallinity (%)	
	D.s.c.	Two-phase model
Undamaged PET	36	30
Damaged PET	40	—

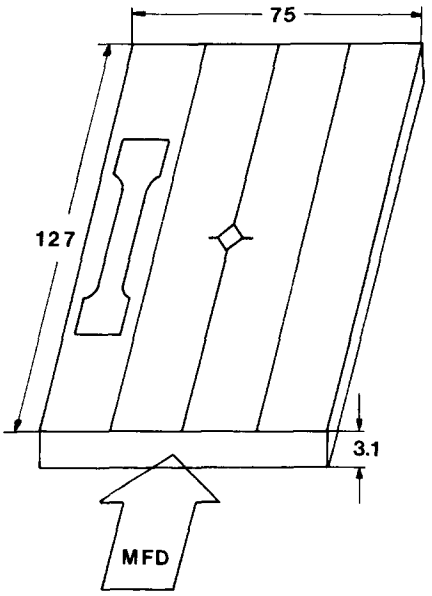

Figure 1 PET plaques, as delivered; position of single edge notched (SEN) and tensile test specimens (MFD is mould fill direction)

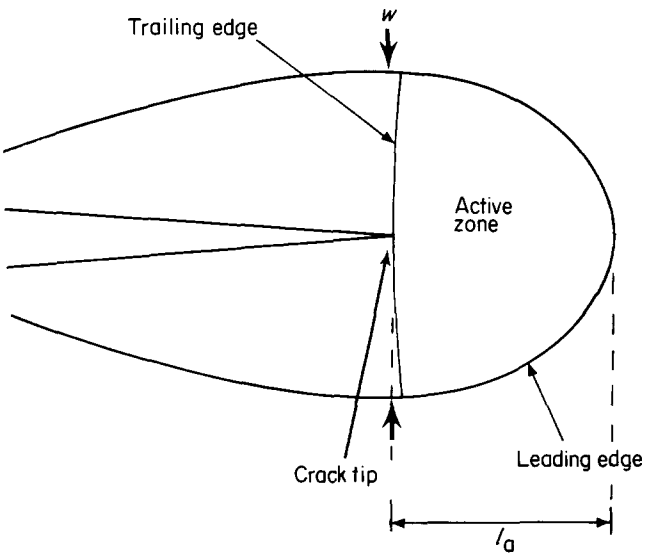

Figure 3 Schematic illustration of CL and the main characteristics of the active zone

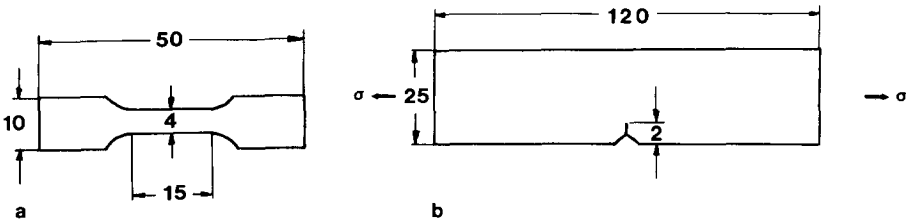

Figure 2 Specimen geometry: (a) tensile test; (b) FCP test

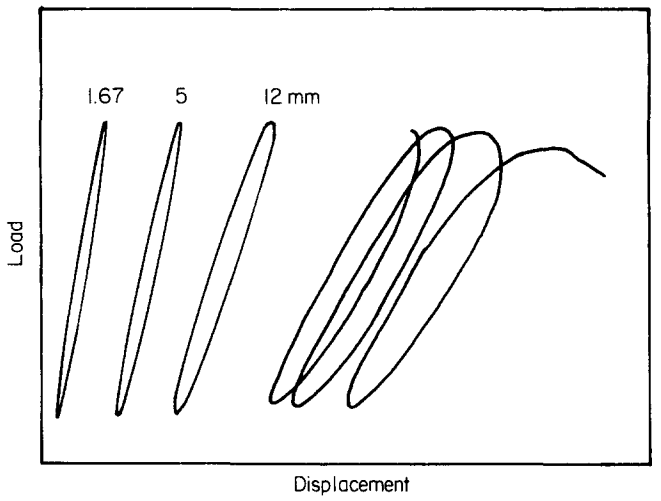

Figure 4 Hysteresis loops at a crack length of 1.67, 5, 12 mm and the last three cycles

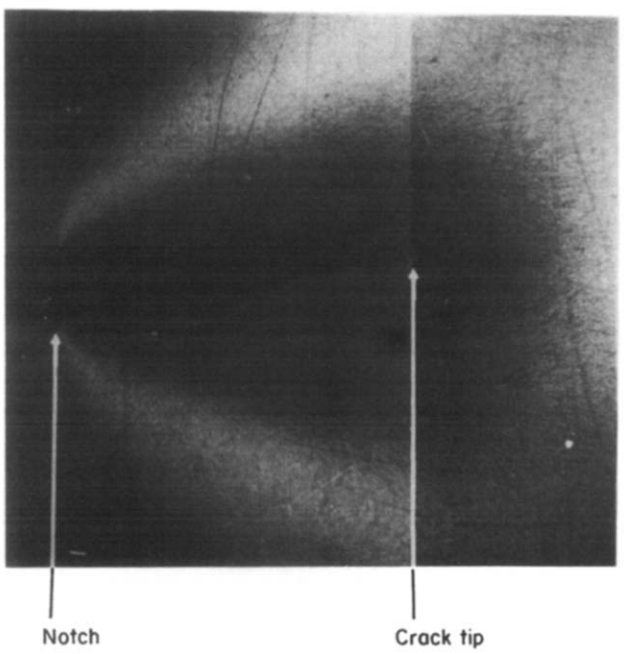

Figure 5 Optical micrograph of the side view

release rate and t_0 is the original specimen thickness. In the following sections a description of the method of data analysis is given.

Crack growth rate (dl/dN)

The actual crack length is obtained from playback of the videotape and plotted against the number of cycles, N. A polynomial curve is fitted through the data. The slope of this curve is the crack growth rate at the corresponding crack length.

Irreversible work (dW_i/dN)

The irreversible work done on the active zone per cycle is experimentally measured by calculating the area within the hysteresis loop associated with each loading–unloading cycle.

Prior to crack propagation ($l = l_0$, where l_0 is the notch length) a finite amount of irreversible work is observed, $W_i(0)$. This is obtained from the area of the loop at the first cycle. As the crack propagates, the area of the loop $W_i(l)$ increases. The total irreversible work done on the active zone per cycle is therefore given by:

$$dW_i/dN = W_i(l) - W_i(0) \tag{3}$$

For illustration, *Figure 4* shows the hysteresis loops of the first cycle and the cycles at $l = 5$, 12 mm and the last three cycles.

Energy release rate evolution

An elastic solution for the energy release rate is no longer applicable, if the active zone is relatively large compared to the crack length and specimen width. The observed active zone (*Figure 5*) is essentially different in size and shape from the predicted plastic zones of the known elastoplastic solutions. Therefore, conventional techniques based on the evolution of load–displacement curves are used for measuring the actual energy release rate[14]. Schematically, this procedure is shown in *Figure 6*. Two load–displacement curves during loading and unloading for two different crack lengths, l_1 and l_2 (with $l_2 > l_1$), are recorded. The area between the two loading curves (shaded by horizontal lines) represents the change in the potential energy (ΔP) for a specific crack advance of $\Delta l = (l_2 - l_1)$. Because unmeasurable crack propagation could take place during loading, the area between the unloading curves (shaded vertically) is a more reliable presentation of ΔP. The ratio of $-\Delta P/\Delta l$ is proportional to the energy release rate corresponding to the intermediate crack length, $l = (l_2 + l_1)/2$. The total energy release rate based on the above procedure can be calculated as:

$$A_1 = \frac{-\Delta P}{\Delta l}\frac{1}{t_0} \tag{4}$$

where t_0 is the original specimen thickness.

Translational resistance moment R_t

In general, the resistance moment R_t is defined as the integral amount of damage formed per unit crack extension. In the case of homogeneous yielding of the active zone, R_t can simply be measured as the volume of

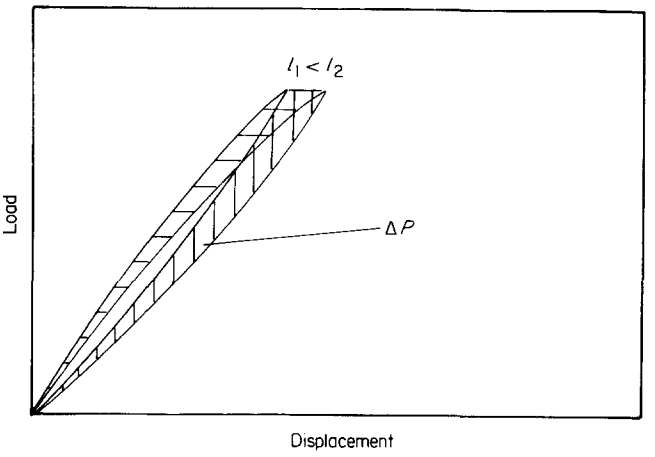

Figure 6 Schematic illustration of the change in potential energy ΔP of the same sample at different crack lengths

transformed material per unit crack extension:

$$R_t = \frac{\Delta V}{t_0 \Delta l}$$

$$\Delta V = \Delta a t(l) \tag{5}$$

where ΔV is the volume of transformed material, Δa is the area of transformed material (*Figure 7*), $t(l)$ is the specimen thickness at $l=(l_2+l_1)/2$ and Δl is the crack propagation (l_2-l_1). As shown in *Figure 7*, the area of transformed material is measured from a side view of the specimen (hatched area). The value of $t(l)$ can be observed from the fracture surface at the corresponding crack length, l.

Specific enthalpy of damage γ^*

In the case of crack instability, a critical crack length, l_c, can be defined. The critical values of the total energy release rate A_{1c} and the translational resistance moment R_{tc} are then obtained. The specific enthalpy of damage is then given as the ratio A_{1c}/R_{tc}. Alternatively[14], γ^* and β may be obtained from the entire crack propagation history, if equation (2) is rewritten in the form:

$$\frac{A_1}{R_t} = -\beta \frac{dW_i/dN}{(dl/dN)R_t t_0} + \gamma^* \tag{6}$$

This equation represents a straight line. The specific enthalpy of damage γ^* is its intercept and the slope is the coefficient β.

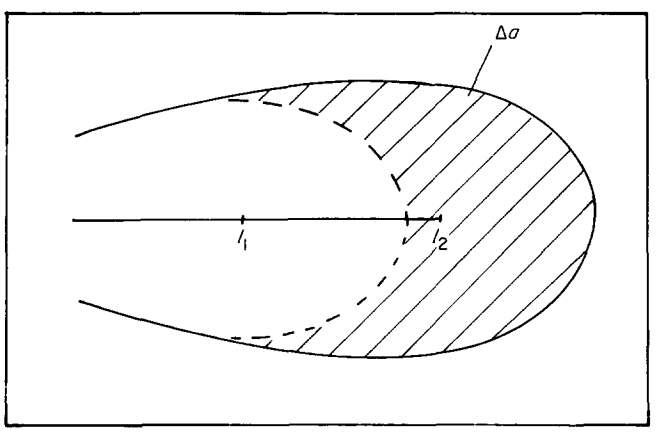

Figure 7 Schematic illustration of the method of measuring the change of transformed material from the specimen side

RESULTS AND DISCUSSION

FCP mechanisms

Figures 5 and *8* are optical micrographs of the side view of a fatigued specimen. The large amount of transformed (yielded) material surrounding the crack tip can be observed.

As described in the literature[1,2], the crack extension in PET is accompanied by yielding, crazes and microcracks beside the crack path and an increase of crystallinity within the damaged material. From the thin sections and the side view of our fatigued specimens, however, no microcracks could be detected. Only an increase of crystallinity from 36% to 40% in the damaged material was observed from d.s.c. analysis (*Table 2*).

The dots in *Figure 8* define one-half of the active zone width as obtained from the videotape. Measurements from cross-sections perpendicular to the crack propagation direction confirmed the active zone, shown in *Figure 9*. From cross-sectional examination, it is noted that 'damage' involves gradual active zone yielding. Maximum active zone yielding at the crack tip was inferred from fracture surface measurements (*Figure 10a*). The normalized specimen thickness plotted *versus* crack length is shown in *Figure 11*. A maximum thinning of 48% of the initial thickness is reached at a 'crack length' of 18 mm. Up to 9 mm crack length, the decrease in thickness is only about 19%. The arrow indicates the 'critical' crack length, which will be explained in the following section. As will be shown later, the 'critical' crack length indicates a transition from fracture to large-scale yielding followed by final rupture. The striations noted on the fracture surface (box A in *Figure 10a* and enlargement of this in *Figure 10b*) appear to indicate the onset of yield instability. The phenomenon is accompanied by large-scale creep, which is reflected in open hysteresis loops (*Figure 4*) towards the ultimate separation of the specimen.

Figures 12a–c are SEM micrographs of the fracture surface taken at crack lengths of 2.5, 9 and 12.5 mm. Obviously, the fracture mechanism becomes more ductile with increasing crack length. This is inferred from the increased drawing of the elementary ligaments after a crack length of 9 mm (*Figures 12b* and *12c*). This transition in the fracture process can also be observed from *Figure 13*. After a crack length of 9 mm, the size of shear lips increases drastically, which lends support to the idea of a transition from fracture to yielding and

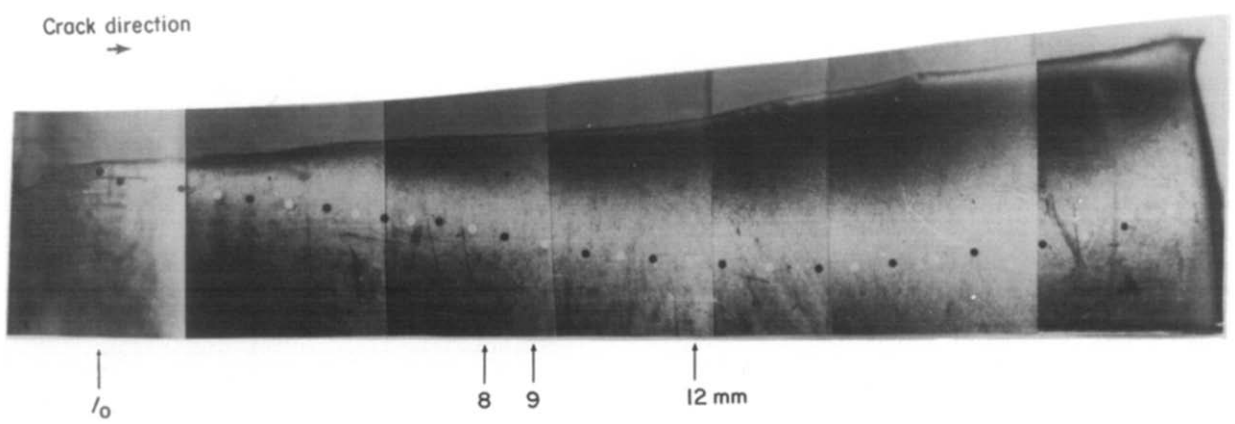

Figure 8 Optical micrograph of the side view of a fatigued specimen. The dots indicate the active zone width

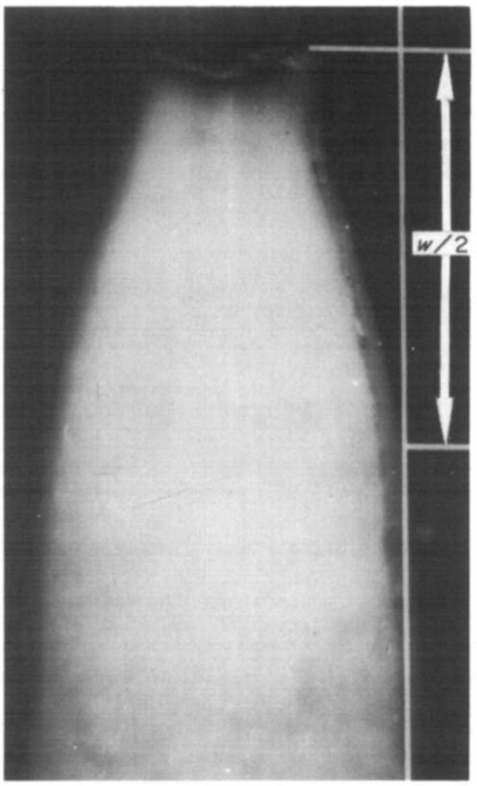

Figure 9 Cross-section perpendicular to the crack path at a crack length of 12 mm

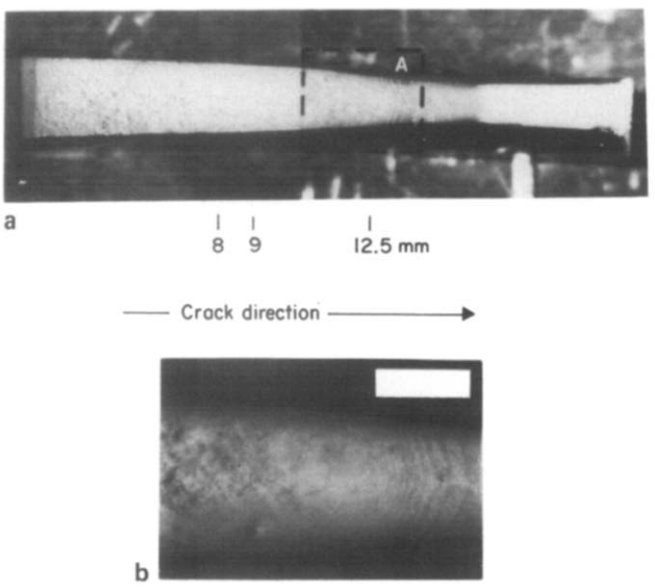

Figure 10 Optical micrograph of the fracture surface: (a) whole specimen; (b) magnification of area A in *Figure 10a*

rupture[15]. Accordingly, a critical crack length, l_c, is defined at a value of $l = 9$ mm. This is not a point of crack instability, as the critical crack length is defined normally in the literature[14]. However, it marks a well defined transitional behaviour in the failure process. After this point, ligament yielding becomes more significant although a measurable crack propagation without an abrupt failure of the sample is observed. In *Figure 14*, the data of crack growth rate are presented as a function of crack length. The arrow indicates the transition from fracture to yielding processes.

In spite of the fact that a transition in the failure mechanism takes place, no remarkable changes in the logarithm of the crack growth rate as a function of crack length (*Figure 14*) is detectable.

Energy release rate

The total energy release rate, A_1, based on the procedure described above is plotted as a function of crack length in *Figure 15*. A_1 represents the change in the potential energy of the specimen during crack propagation and simultaneous damage advance. The arrow indicates the 'critical' crack length, as defined

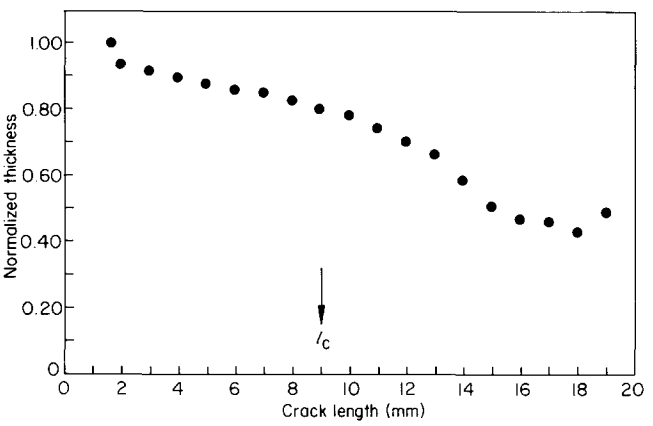

Figure 11 Normalized thickness as a function of crack length (l_c is critical crack length)

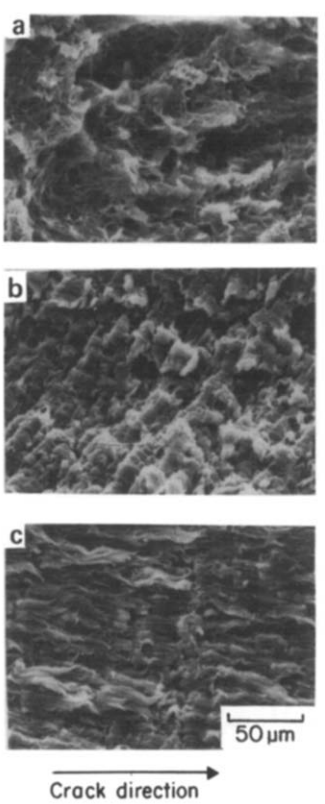

Figure 12 SEM micrographs of the fracture surface at different crack lengths: (a) typical fractographic morphology of slow fracture at $l = 2.5$ mm (area A in *Figure 13*); (b) fracture surface appearance at the transition from slow to fast fracture ($l = 9$ mm, area B in *Figure 13*); (c) yielding during FCP at a crack length of 12.5 mm (area C in *Figure 13*)

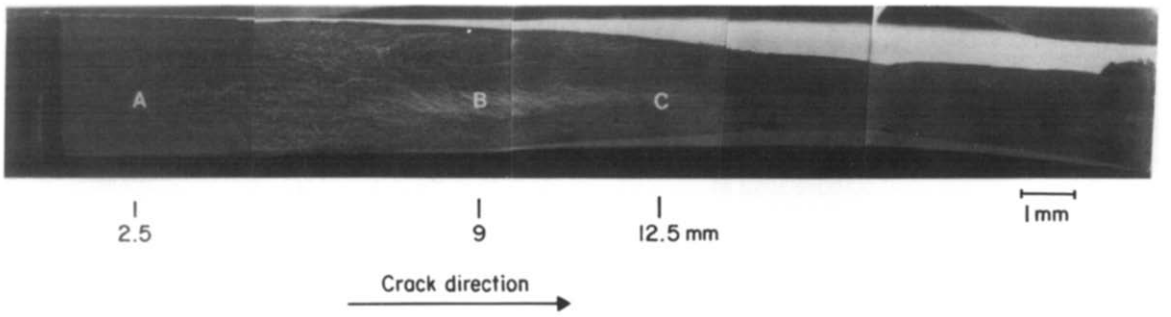

SEM micrograph of the fracture surface

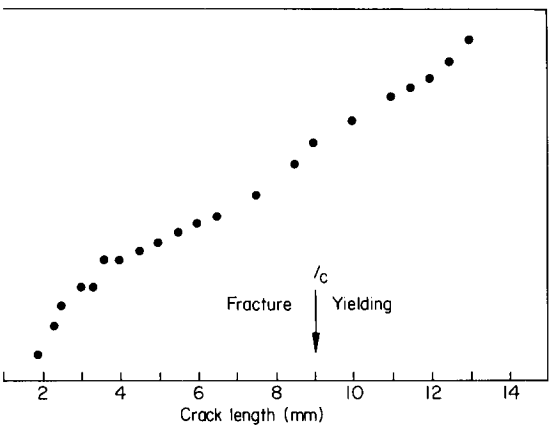

Crack growth rate as a function of crack length

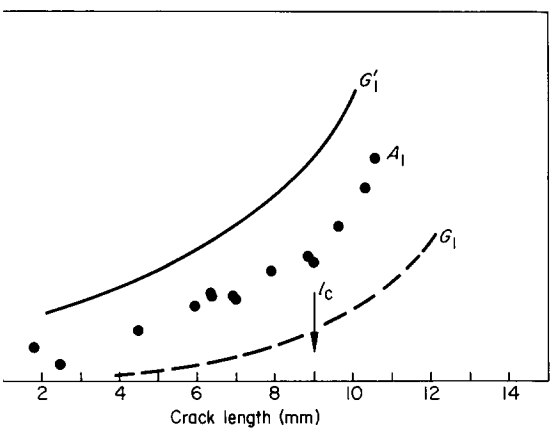

Total energy release rate A_1 as a function of crack length, to G_1 and G_1'

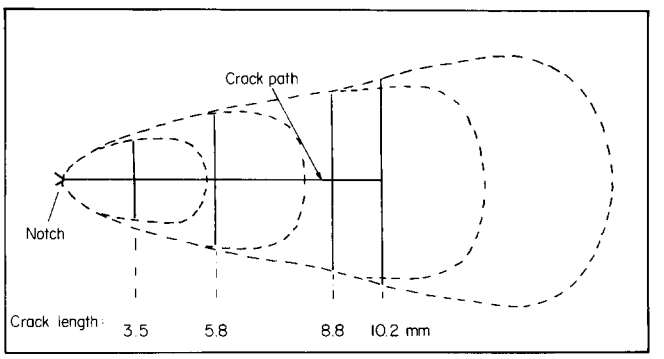

Figure 16 Evolution of the active zone during stable crack propagation. The full line represents the crack path

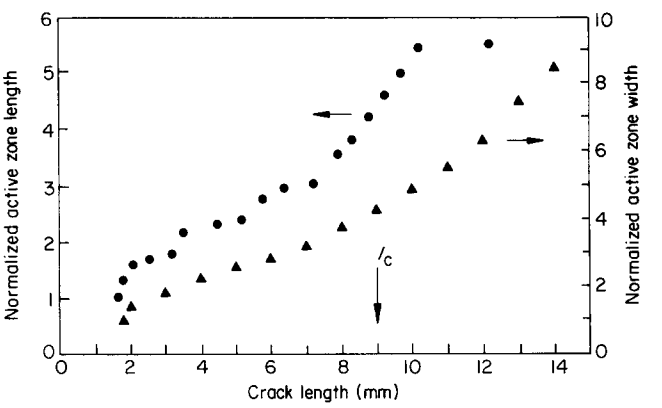

Figure 17 Normalized active zone length, l_a/l_{a0} (●), and width, w_a/w_{a0} (▲), as functions of crack length

t this point a 'critical' energy release rate $A_{1c}=$ $^{-2}$ can be obtained.

broken curve shows the energy release rate d from the linear elastic relationship:

$$G_1=(K_I^2/E)(1-\nu^2) \quad (7)$$

$_I$ is the stress intensity factor[16], E is the elastic s and ν is the Poisson ratio. The solid curve its the energy release rate, G_1', accounting for plastic zone correction[17]. Here, the actual active igth, l_a, is taken as the plastic zone size for the ion of G_1'. Both curves have similar shapes to the ergy release rate curve A_1. However, neither G_1 give a good approximation to the measured A_1.

Resistance moment

The evolution of the active zone during stable crack growth is depicted in *Figure 16*. A few crack layer configurations are presented. These are traced from video playbacks. Obviously, the amount of yielded material adjacent to the crack tip increases with increasing crack length. This causes an increase of energy absorption with crack length.

The active zone width w and its length l_a (*Figure 3*) provide a quantitative measure of damage evolution at the crack tip. Prior to measurable crack propagation, an active zone, whose length is l_{a0} and whose width is w_0, develops. The ratios (l_a/l_{a0}) and (w/w_0) as functions of crack length are shown in *Figure 17*. It is obvious that the active zone length and width evolve generally in a similar fashion, indicating geometric similarity. In addition, it is clear that the active zone becomes markedly enlarged past

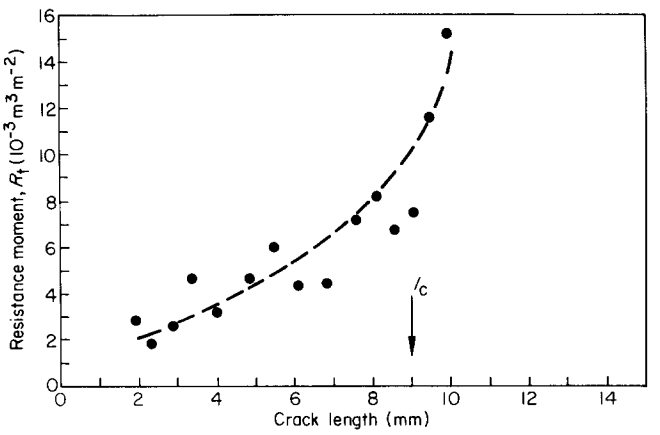

Figure 18 Resistance moment as a function of crack length

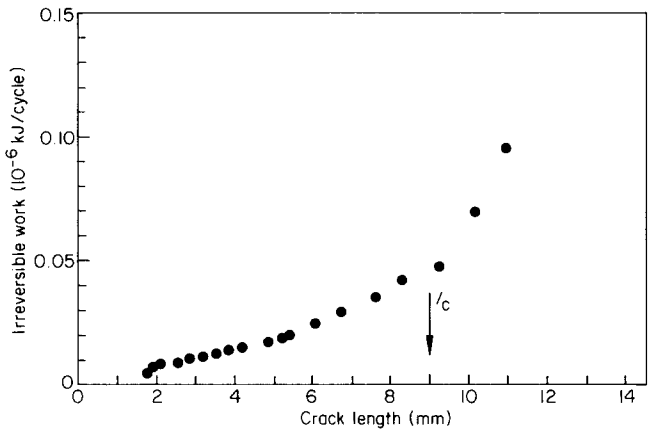

Figure 19 Irreversible work as a function of crack length

l_c. This observation supports our contention of a transition from fracture to large-scale yielding.

Owing to the fact that the damage during FCP in our crystalline PET involves yielding, the resistance moment, R_t, can be calculated in terms of equation (5). The results are shown in *Figure 18*. Here R_t is plotted as a function of crack length. Up to l_c, a nearly linear increase of R_t can be observed. Past l_c, however, the resistance moment increases excessively. The critical value of R_t at the transition point l_c is about $R_{tc} = 8.9 \times 10^{-3}$ m^3 m^{-2} (that is in cubic metres of transformed (yielded) material per square metre of crack plane advance).

Irreversible work

According to the procedure described above, the irreversible work done on damage creation within the active zone is determined. The results are presented in *Figure 19* as a function of crack length. The values of dW_i/dN could only be calculated up to $l = 11$ mm. This is due to the fact that after this crack length is reached, excessive creep during loading occurs, thus opening the hysteresis loops (*Figure 4*).

Specific enthalpy of damage and dissipation coefficient

From the early crack propagation history, γ^* and β are calculated in terms of equation (6). In *Figure 20* A_1/R_t is plotted as a function of $(dW_i/dN)[(dl/dN)R_t t_0]^{-1}$. Actually, the data show a very good linear behaviour in the crack length range from 3 to 8 mm. Linear regression is employed to fit these data. The intercept of the straight line yields a specific enthalpy of damage $\gamma^* = 2200$ kJ m^{-3}. This value appears to be lower than that reported for polycarbonate[6] ($\gamma^* = 76$ MJ m^{-3}) and for high-density polyethylene[14] ($\gamma^* = 4000$ kJ m^{-3}).

The dissipation coefficient β is calculated from the slope as $\beta = 7.3 \times 10^{-5}$. This indicates that the major part of dissipation $(1-\beta)$ occurred as heat.

Although the proposed fracture-to-yielding transition is conceptually different from the well defined critical crack propagation transition, it is tempting to assess γ^* as A_{1c}/R_{tc}. Such a value for γ^* is found to be about 1900 kJ m^{-3}. The close similarity between this value and that obtained from the entire crack propagation (fracture) history, i.e. $\gamma^* = 2200$ kJ m^{-3}, strengthens the rationale of the proposed transition.

Employing the values of $\gamma^* = 2200$ kJ m^{-3} and $\beta = 7.3 \times 10^{-5}$ in addition to the obtained data of A_1, R_t and dW_i/dN, the rate of crack propagation is calculated using equation (2). In *Figure 21* a comparison between calculated and measured crack growth rate is presented. The calculated data are in very good agreement with the measured values. This shows the applicability of the crack layer theory for describing the entire crack propagation history.

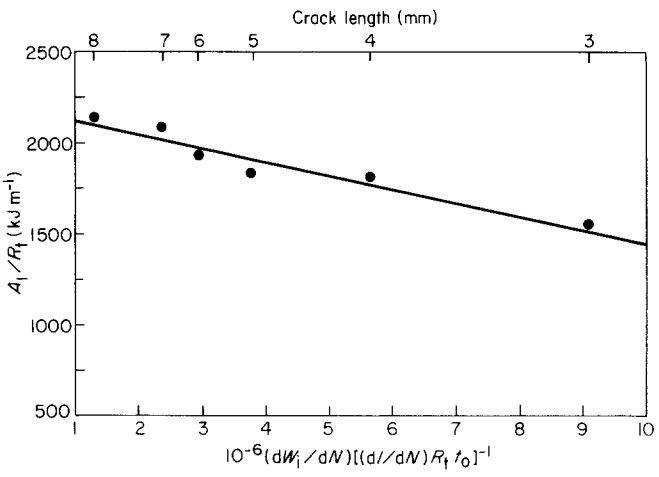

Figure 20 Determination of γ^* and β ($\gamma^* = 2200$ kJ m^{-3}, $\beta = -7.3 \times 10^{-5}$)

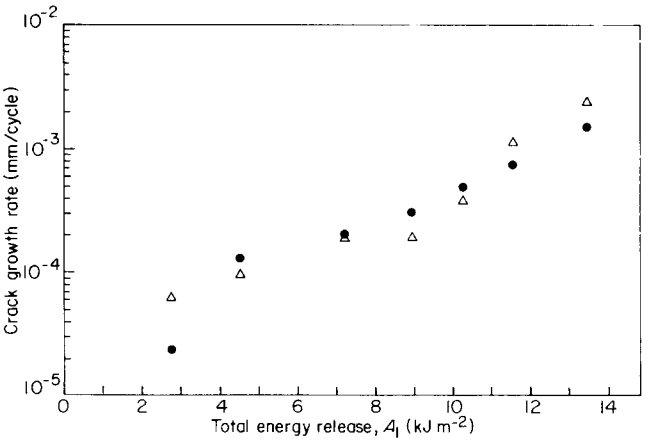

Figure 21 Comparison between calculated (△) and experimentally obtained (●) crack growth rates as a function of A_1

CONCLUSIONS

Fatigue crack propagation in crystalline PET is accompanied by an increasing damage zone around the crack tip. This damage is characterized as a yielding process and an increase of crystallinity.

A change in FCP behaviour from a fracture process to a yielding process is suggested in the absence of conventional crack instability.

From the crack layer theory, the specific enthalpy of damage (recrystallization) is found to be in the region of 2000 kJ m^{-3}. The predicted crack growth rate, calculated in terms of the crack layer equation, is in good agreement with the measured crack propagation data.

ACKNOWLEDGEMENTS

The material was supplied by E.I. de Pont de Nemours & Co. Inc., Wilmington, DE, USA. The authors would like to thank Mr Michael Napolitano for the d.s.c. measurements. Personal communications with Dr M. Kasakevich were very helpful.

REFERENCES

1 Ramires, A., Mason, J. A. and Hertzberg, R. W. *Polym. Eng. Sci.* 1982, **22**, 975
2 Friedrich, K. 'Fracture Mechanical Behavior of Short Fiber Reinforced Thermoplastics', Fortschr.-Ber. VDI-Z, Reihe 18, No. 18, 1984
3 Paris, P. C. Report No. 62-Met-3, ASME, New York, 1968
4 Chudnovsky, A. 'The Crack Layer Theory', NASA Report, Case Western Reserve University, Cleveland, Ohio, 1983
5 Chudnovsky, A. and Moet, A. *J. Mater. Sci.* 1985, **20**, 630
6 Haddaoui, N., Chudnovsky, A. and Moet, A. *Polymer* 1986, **27**, 1377
7 Wang, X., Sehanobish, K. and Moet, A. *Polym. Compos.* in press
8 Chudnovsky, A., Moet, A., Bankert, R. J. and Takemori, M. T. *J. Appl. Phys.* 1983, **54**, 5562
9 Friedrich, K. 'Microstructure and Fracture of Fiber Reinforced Thermoplastic PET', Fortschr.-Ber. VDI-Z, Reihe 18, No. 12, 1982
10 van Krevelen, D. W. 'Properties of Polymers', Elsevier, Amsterdam, 1976
11 Samuels, R. J. 'Structural Polymer Properties', Wiley, New York, 1974
12 Garg, S. K. *J. Appl. Polym. Sci.* 1982, **27**, 2857
13 Manson, J. A. and Hertzberg, R. W. 'Fatigue of Engineering Plastics', Academic Press, New York, 1980
14 Sehanobish, K., Chudnovsky, A. and Moet, A. *Polymer* 1987, **28**, 1315
15 Takemori, M. T. *Polym. Eng. Sci.* 1982, **22**, 937
16 Tada, H., Paris, P. C. and Irwin, G. R. 'The Stress Analysis of Cracks Handbook', Del Research Corporation, Hellertown, PA, 1973
17 Irwin, G. R. *Appl. Mater. Res.* 1964, **3**, 65